Observation of self-mode-locking assisted by high-order transverse modes in optically pumped semiconductor lasers

2014 Laser Phys. Lett. 11 105803

(http://iopscience.iop.org/1612-202X/11/10/105803)

IOP Publishing | Astro Ltd
Laser Physics Letters
Laser Phys. Lett. **11** (2014) 105803 (7pp)
doi:10.1088/1612-2011/11/10/105803

Observation of self-mode-locking assisted by high-order transverse modes in optically pumped semiconductor lasers

H C Liang[1], C H Tsou[2], Y C Lee[2], K F Huang[2] and Y F Chen[2,3]

[1] Institute of Optoelectronic Science, National Taiwan Ocean University, Keelung 20224, Taiwan
[2] Department of Electrophysics, National Chiao Tung University, 1001 Ta-Hsueh Rd. Hsinchu 30010, Taiwan
[3] Department of Electronics Engineering, National Chiao Tung University, 1001 Ta-Hsueh Rd. Hsinchu 30010, Taiwan

E-mail: yfchen@cc.nctu.edu.tw

Received 7 March 2014, revised 8 August 2014
Accepted for publication 14 August 2014
Published 15 September 2014

Abstract
The criterion for achieving the self-mode-locking (SML) in an optically pumped semiconductor laser (OPSL) with a linear cavity is systematically explored. Experimental results reveal that the occurrence of SML can be assisted by the existence of high-order transverse modes. Numerical analysis is performed to confirm that the critical pump power for obtaining the SML operation agrees very well with the pump threshold for exciting $TEM_{1,0}$ mode. The present finding offers an important insight into laser physics and a useful indication for obtaining the SML operation in OPSLs.

Keywords: self-mode-locking, optically pumped semiconductor lasers, transverse modes

(Some figures may appear in colour only in the online journal)

1. Introduction

The occurrence of self-mode-locking (SML) is an intriguing phenomenon in a laser system without any saturable absorbers. Since Spence *et al* first demonstrated SML in the Ti-sapphire laser [1], the phenomena of Kerr-lens mode locking (KLM) have been widely explored both experimentally and theoretically [2–6]. Recently, numerous SML lasers have been demonstrated for the Nd-doped [7–9] and Yb-doped [10–14] gain media in linear short cavities without saturable absorbers. So far, the origin of the self-mode-locking is conjectured to result from the combined effects of the Kerr lensing and thermal lensing [8, 9, 12, 14]. In addition to solid-state crystal lasers, the SML operation has also been demonstrated in the optically pumped semiconductor lasers (OPSLs [15–17]). However, the requirement for achieving SML in OPSLs has not actually been discovered yet. Furthermore, since carrier dynamics in semiconductor gain media can affect the phase locking between lasing modes, clarifying the difference between the criteria for achieving SML in solid-state lasers and semiconductor lasers is scientifically important in laser physics.

The formation of transverse modes always plays a significant role in the temporal dynamics of lasers. In end-pumped lasers, the pump-to-mode size ratio predominantly not only determines the pump threshold for TEM_{00} but also affects the pump threshold for other high-order transverse modes. In this work, we design various pump-to-mode size ratios in an OPSL with a plano-concave cavity to explore the performance of SML. We systematically measure the critical pump power for achieving the SML varying with the pump-to-mode size ratio. We experimentally find that as the pump-to-mode size ratio is less than 1.5, the critical pump power significantly increases to be far above the lasing threshold. We further employ the theoretical formula and experimental parameters to confirm that the critical pump power for obtaining the SML operation agrees very well with the pump threshold for exciting $TEM_{1,0}$ mode. The good agreement implies that the existence of high-order transverse modes can assist the phase locking between lasing longitudinal modes. More importantly, the

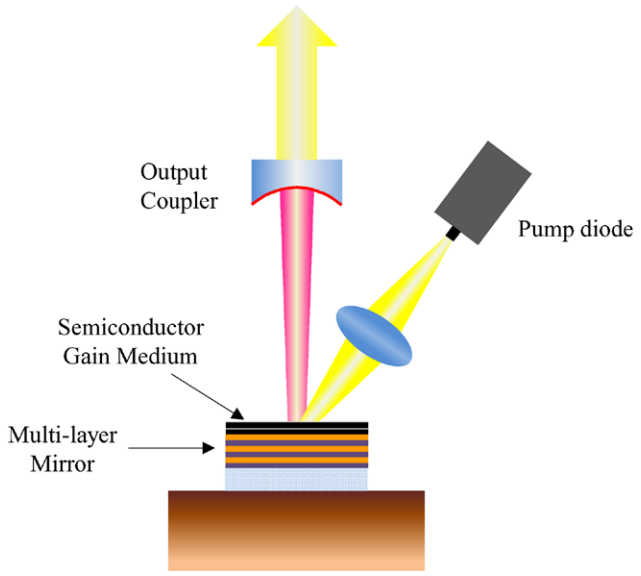

Figure 1. Experimental setup for exploring the SML performance in an OPSL.

present finding can provide an important route for fulfilling SML in OPSLs.

2. Experimental set-up

Figure 1 depicts the experimental scheme for exploring the SML performance in an OPSL. The laser cavity consists of a concave mirror, a semiconductor gain chip and a pump laser diode. The gain chip was obtained from a commercial OPSL module (Coherent Inc.). The gain chip included a structure of distributed Bragg reflectors (DBRs) to form a front mirror and a structure of multiple quantum wells to form a resonant periodic gain. The photoluminescence emission wavelength of the gain chip was approximately 1060 nm at room temperature. The gain chip was soldered with indium to a chemical vapour deposition diamond heat spreader with DBR side down for effectively removing the heat from the gain structure. For convenience, the cavity length $L_{\rm cav}$ was set to be 83 mm in experiment. The radius of the pump beam ω_p was approximately 320 μm. Several concave output couplers with the radius of curvature $R_{\rm oc}$ ranging from 100 mm–1000 mm were used to explore the variation of the lasing threshold and the influence of pump-to-mode size ratios on the pump critical power for achieving the SML operation. The output transmission for all output couplers was 2%. With ABCD matrix, the cavity mode size on the gain chip is given by

$$\omega_l = \sqrt{\frac{\lambda}{\pi}\sqrt{L_{\rm cav}\left(R_{\rm oc} - L_{\rm cav}\right)}}\ . \qquad (1)$$

With equation (1), it can be found that changing $R_{\rm oc}$ from 100 mm–1000 mm leads the cavity mode size to vary from 117 μm–303 μm for $L_{\rm cav}$ = 83 mm and λ = 1064 nm. As a result, the pump-to-mode size ratio ω_p/ω_l can be adjusted in the range of 1.06–2.74 for ω_p = 320 μm. The temporal dynamics was detected by a high-speed InGaAs photodetector (Electro-Optics Technology Inc. ET-3500 with rise time 35 ps), whose output signal was connected to a digital oscilloscope (Agilent DSO80000) with 10 GHz electrical bandwidth and a sampling interval of 25 ps. A Fourier optical spectrum analyzer (Advantest Q8347), which was constructed with a Michelson interferometer, was employed to monitor the spectral information with the resolution of 0.002 nm.

3. Experimental results

First of all, we used $R_{\rm oc}$ = 300 mm to investigate the temporal dynamics varying with the pump power. Under this condition, the pump-to-mode size ratio ω_p/ω_l was 1.51 and the lasing threshold was experimentally found to be approximately 5.0 W. Figure 2 shows experimental results for RF power spectra measured at four different pump powers. For the pump power ranging from lasing threshold to 9.5 W, the lasing state was in the continue-wave (CW) operation and there were no obvious peaks which appeared in the RF spectrum, as shown in figure 2(*a*) for the result measured at a pump power of 7 W. Figure 3 shows overall performances for the laser operated in the CW state. The transverse pattern was rather circularly symmetric, as seen in figure 3(*a*). The temporal traces measured with a 10 GHz bandwidth real-time oscilloscope did not reveal any obvious oscillations, as seen in figure 3(*b*). The full width at half maximum (FWHM) in the optical spectrum was found to be as narrow as 0.1 nm, as shown in figure 3(*c*).

For the pump power in the rather small range of 9.5–10.0 W, the temporal trace in the oscilloscope revealed the laser to be in an intermittent mode-locked state and there were several peaks which appeared in the RF spectrum. The peak frequencies corresponded to the harmonics of the longitudinal mode spacing $f_{\rm L}$ = 1.8 GHz, as shown in figure 2(*b*). Since the mode-locked pulse train was discontinuous, the peak values in the RF spectrum were generally less than 20 dBm, considerably smaller than the standard value of well-behaved mode-locked lasers. For the pump power greater than 10.0 W, the temporal trace in the oscilloscope displayed the laser to be in a continuous mode-locked state and the structure of the pulse train was spatially dependent. Meanwhile, there were two beat peaks which accompanied the harmonics of the longitudinal mode spacing in the RF spectrum, as shown in figure 2(*c*) for the result measured at a pump power of 11.5 W. The beat frequency was measured to be 375 MHz which exactly corresponded to the transverse mode spacing f_T. When the pump power was up to 15 W, the overall temporal behaviour was found to be unchanged, as shown in figure 2(*d*). The spatial dependence of the mode-locked pulse train and the appearance of the beat peaks at the frequencies of $f = mf_L \pm f_T$ with m =1, 2, 3 in the RF spectrum clearly indicated that the first high-order transverse mode had been generated. Experimental results imply that the presence of the high-order transverse modes is intimately associated with the emergence of a long-lasting SML operation. It is worthwhile to mention that this association is absent from the SML solid-state lasers [7–9].

Figure 4 shows overall performances for the laser operated in the mode-locked state. The transverse pattern became elliptical and the temporal trace in the centre of the transverse pattern displayed full modulation without any CW background, as

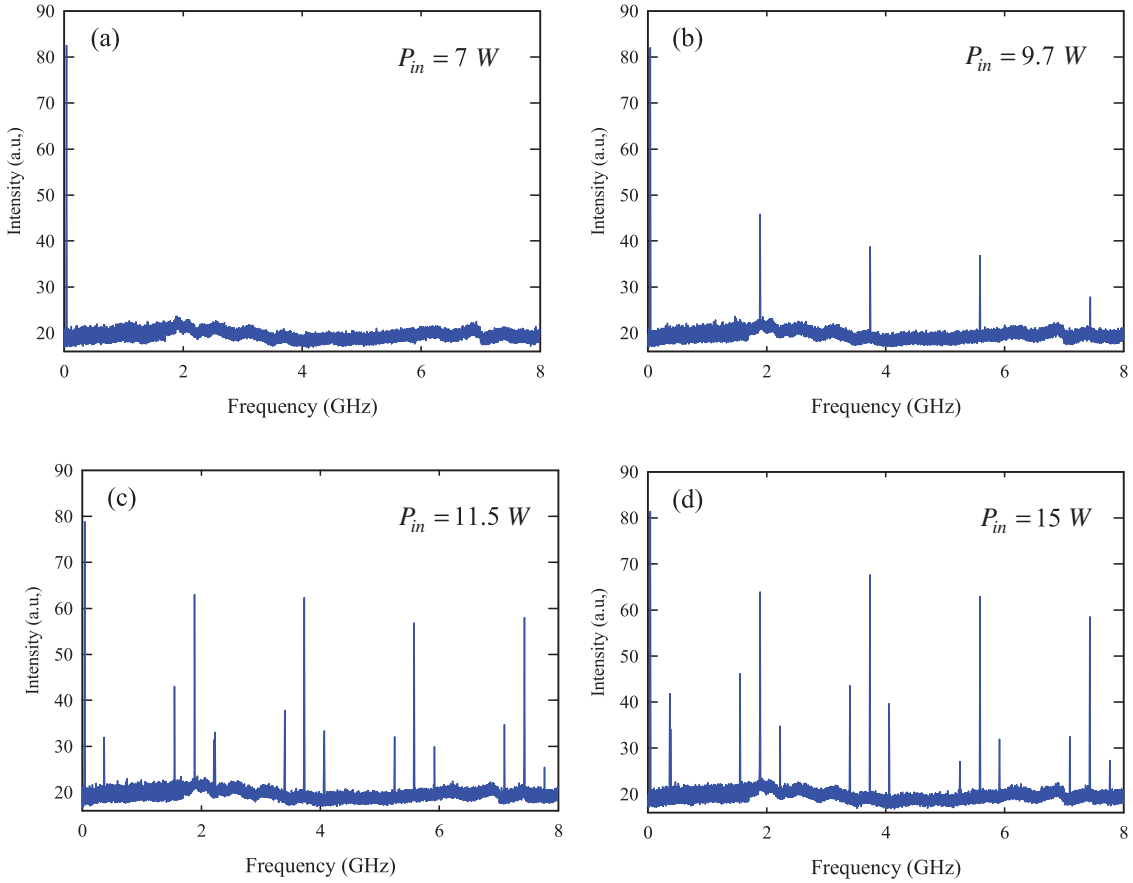

Figure 2. Experimental results for RF power spectra measured at different pump powers: (*a*) P_{in} =8 W, (*b*) P_{in} = 9.7 W, (*c*) P_{in} = 11.5 W, (*d*) P_{in} = 15 W.

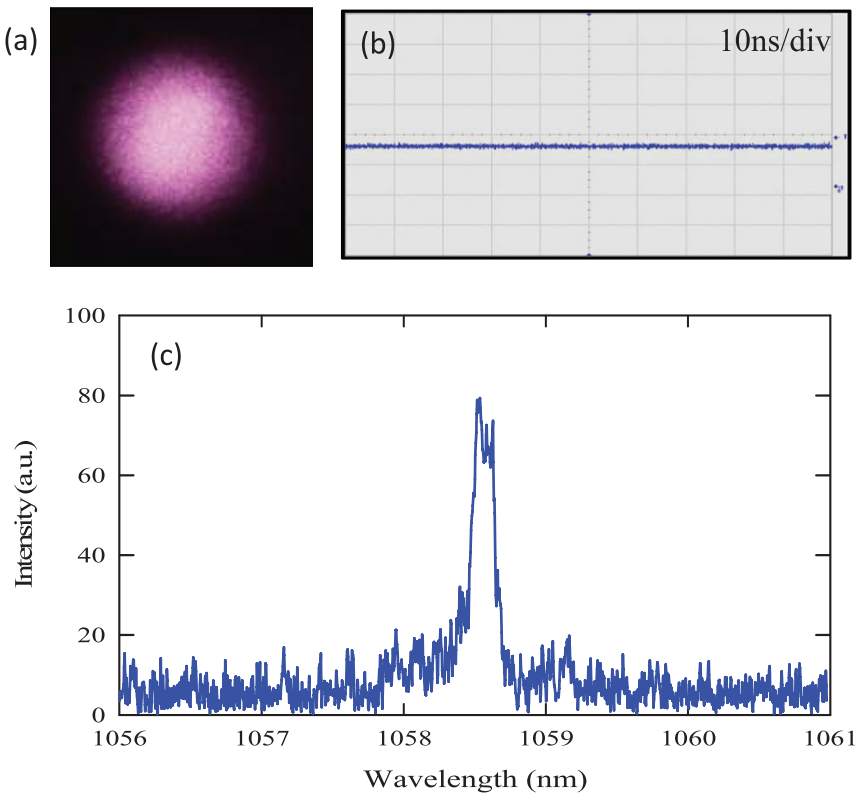

Figure 3. Experimental measurements for overall performances of the laser operated in the CW state: (*a*) transverse pattern, (*b*) temporal trace, (*c*) optical spectrum.

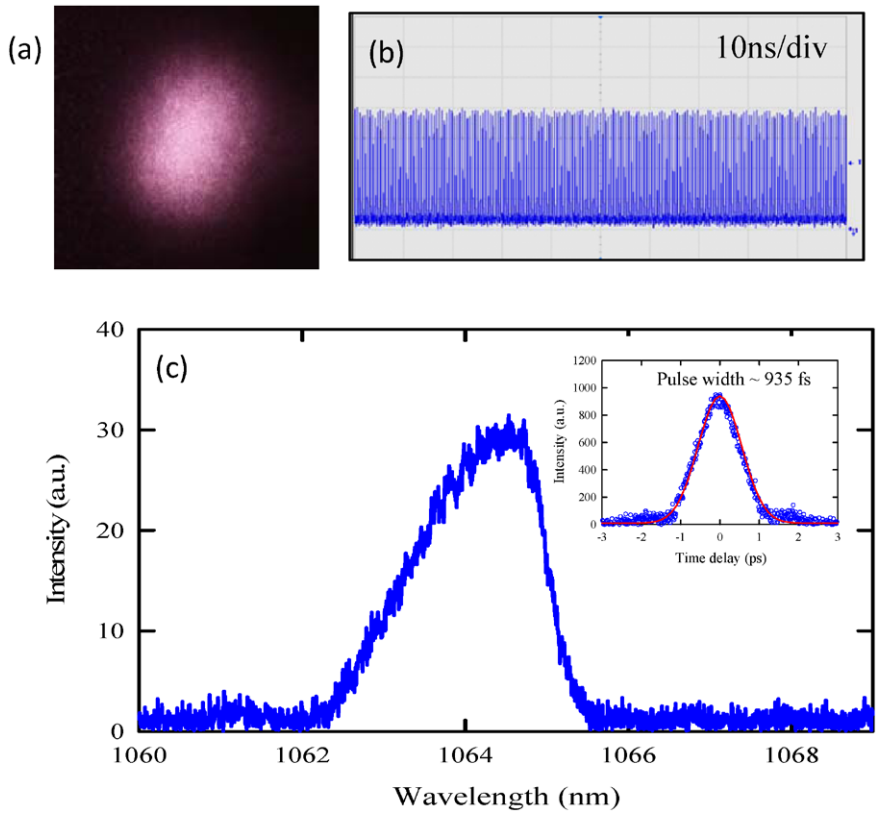

Figure 4. Experimental measurements for overall performances of the laser operated in the mode-locked state: (*a*) transverse pattern, (*b*) temporal trace, (*c*) optical spectrum and the inset for auto-correlation trace.

shown in figures 4(*a*) and (*b*), respectively. Note that the temporal traces in the position out of the beam center were generally found to be modulated with the transverse beat frequency. This spatiotemporal dynamics is attributed to the simultaneous longitudinal and transverse mode locking [18]. The full width at half maximum (FWHM) in the optical spectrum was found to be as wide as 1.8 nm, as shown in figure 4(*c*). The pulse width for the mode-locked pulse train was measured with an autocorrelator (APE pulse check, Angewandte Physik & Elektronik GmbH). Assuming the Gaussian-shaped temporal profile, the FWHM of the pulse was approximately 935 fs, as shown in the inset of figure 4(*c*). As a result, the time-bandwidth product was approximately 0.446, which was close to the Fourier-limited value.

We further exploited the variation of the peak amplitude at $f = f_L$ in the RF spectrum with the pump power to identify the critical pump P_{SML} for achieving the SML operation. Figure 5 depicts experimental results for the peak amplitude at $f = f_L$ versus the pump power. It is clear that there is a rapid increase at a pump power near 10.0 W. For quantitative analysis, the critical pump power P_{SML} is defined to be the pump power at which the peak amplitude at $f = f_L$ starts to exceed 40 dBm.

Following the same experimental procedure, we explored the variation of the critical pump power P_{SML} with the pump-to-mode size ratios ω_p/ω_l by using different concave output couplers. Figure 6 shows experimental results for the average output power versus the pump power obtained with different pump-to-mode size ratios, where the CW and SML regions are specified by the critical pump power P_{SML}. It can be seen

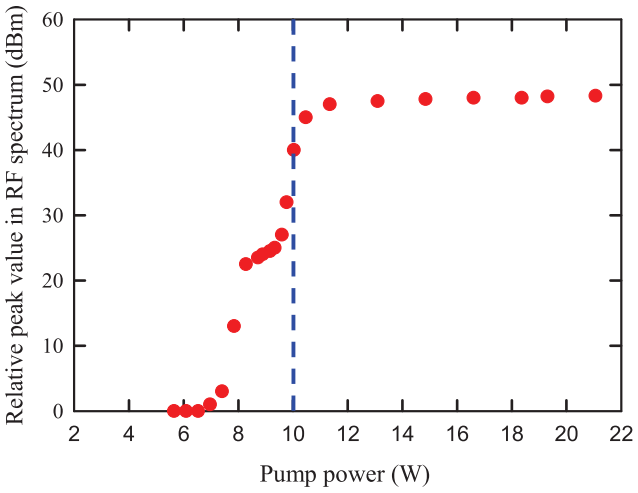

Figure 5. Experimental results for the pump-power dependence of the peak amplitude at $f = f_L$ in the power spectrum.

that decreasing the pump-to-mode size ratio leads to a significant increase in the critical pump power for achieving SML. Furthermore, experimental results revealed in the same way that when the pump power began to be higher than the critical pump power P_{SML}, there were transverse beat components to accompany every harmonic peak of the longitudinal mode spacing in the RF spectrum. All experimental observations indicated that the existence of high-order transverse modes can assist the phase locking between longitudinal modes to achieve the SML operation. As a result, the critical pump power P_{SML}

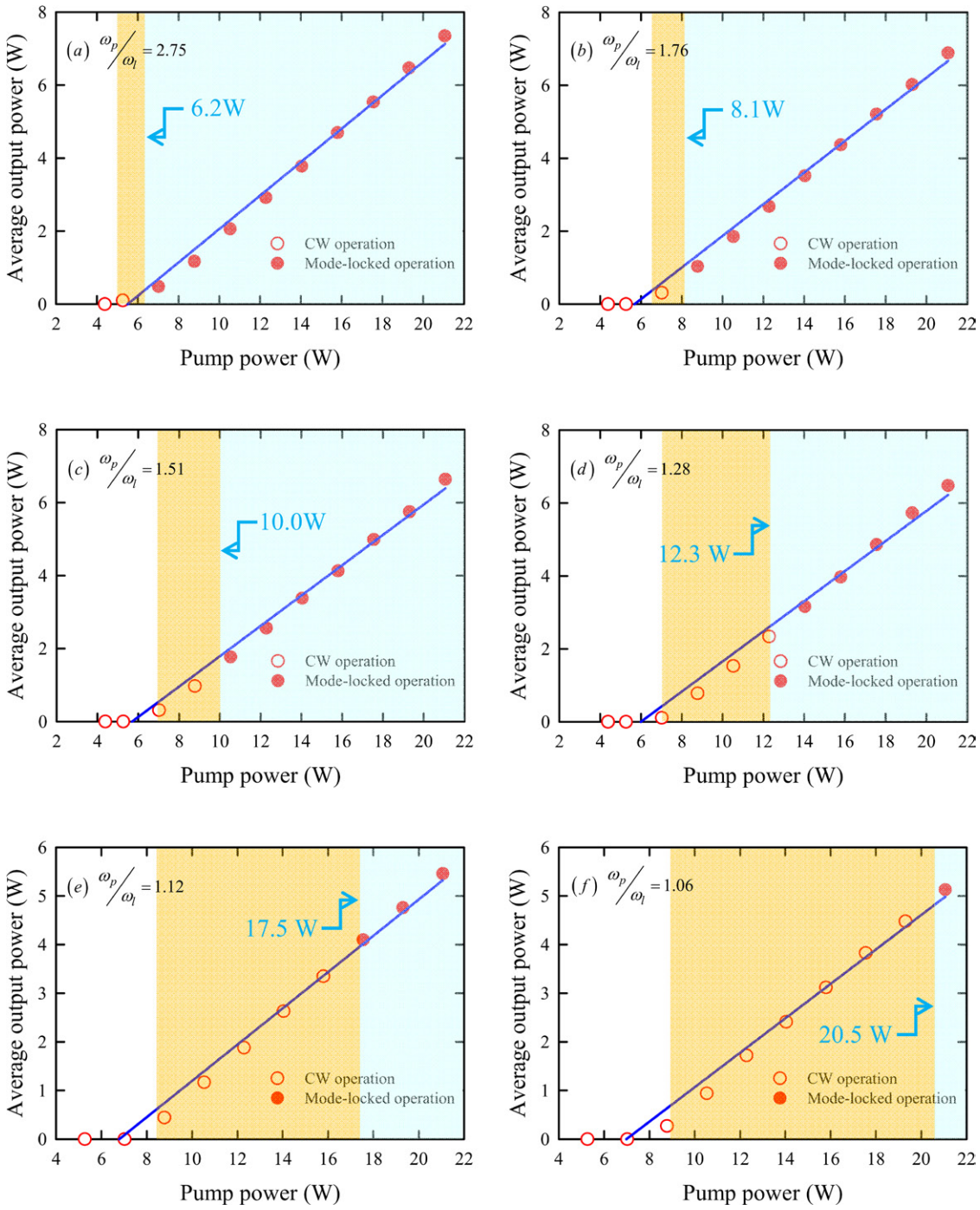

Figure 6. Experimental results for the average output power versus the pump power obtained with different R_{oc} for different pump-to-mode ratios: (*a*) $\omega_p/\omega_l = 2.75$, (*b*) $\omega_p/\omega_l = 1.76$, (*c*) $\omega_p/\omega_l = 1.51$, (*d*) $\omega_p/\omega_l = 1.28$, (*e*) $\omega_p/\omega_l = 1.12$, (*f*) $\omega_p/\omega_l = 1.06$. The critical pump power P_{SML} used to specify the CW and SML regions.

for attaining SML can be forecasted from the pump threshold for high-order transverse modes. In the following, we perform a numerical calculation to confirm this feasibility.

4. Numerical analysis

Kuznetsov *et al* [19] have successfully developed a theoretical model to analyze the pump threshold for the fundamental transverse mode. Here, we apply the effective mode area to this theoretical model to calculate the pump thresholds for various $TEM_{n,0}$ modes. The effective mode area for $TEM_{n,0}$ mode can be obtained with the overlap integral [20]:

$$A_{n,0} = \left(\int\int s_{n,0}(x,y)\, r_p(x,y)\, \mathrm{d}x\mathrm{d}y \right)^{-1}, \qquad (2)$$

where $s_{n,0}(x,y)$ is the normalized cavity mode distribution and $r_p(x,y)$ is the normalized pump distribution. For $TEM_{n,0}$ mode, $s_{n,0}(x,y)$ is given by

$$s_{n,0}(x,y) = \frac{2}{\pi\omega_l^2 2^n n!} H_n^2\left(\frac{\sqrt{2}x}{\omega_l}\right)\exp\left[-\frac{2(x^2+y^2)}{\omega_l^2}\right], \quad (3)$$

where $H_n()$ is the Hermite polynomial of order n. The normalized pump distribution $r_p(x,y)$ is approximated as a Gaussian distribution:

$$r_p(x,y) = \frac{2}{\pi\omega_p^2}\exp\left[-\frac{2(x^2+y^2)}{\omega_p^2}\right]. \quad (4)$$

Substituting equations (3) and (4) into equation (2), after some algebra, the effective mode area can be analytically integrated as

$$A_{n,0} = \frac{\pi{\omega_p}^2}{2}\frac{1}{\sum_{k=0}^{n}\frac{n!}{2^{2(n-k)}k!}\left(\frac{\xi}{1+\xi}\right)^{k+1}\left\{\sum_{j=0}^{[(n-k)/2]}\frac{H_{n-k-2j}(0)}{j!(n-k-2j)!}\left(\frac{\xi-1}{\xi+1}\right)^{j}\right\}^2}, \quad (5)$$

where $\xi = \left(\omega_p / w_l\right)^2$. In terms of the effective mode area, the pump threshold for the single $\mathrm{TEM}_{n,0}$ mode oscillation can be given by [19]

$$P_{\mathrm{th}}(\mathrm{TEM}_{n,0}) = n_{\mathrm{th}}\frac{h\nu N_w L_w}{\eta_{\mathrm{abs}}\tau(n_{\mathrm{th}})}A_{n,0}, \quad (6)$$

where $h\nu$ is the photon energy, η_{abs} is the pump absorption efficiency, N_w is the number of quantum wells, L_w is the quantum well thickness. The carrier life time $\tau(n)$ and the threshold carrier density n_{th} are given by

$$\frac{1}{\tau(n)} = A + Bn + Cn^2 \quad (7)$$

and

$$n_{\mathrm{th}} = n_0\left(\frac{1}{R_1 R_2 T_{\mathrm{loss}}}\right)^{(2\Gamma g_0 N_w L_w)^{-1}}, \quad (8)$$

respectively. Here n_0 is the transparency carrier density, R_1 and R_2 are the reflectivity of cavity mirrors, g_0 is the material-gain parameter, Γ is the longitudinal confinement factor, T_{loss} is the transmission factor due to the round-trip loss, A, B and C are the monomolecular, bimolecular, and Auger recombination coefficients.

With equations (5)–(8), we calculated the pump thresholds for $\mathrm{TEM}_{0,0}$ and $\mathrm{TEM}_{1,0}$ modes. According to the experimental condition, the parameters used in the calculation were as follows: $\eta_{\mathrm{abs}} = 0.85$, $L_w = 8$ nm, $N_w = 10$, $N_0 = 1.7\times10^{18}\,\mathrm{cm}^{-3}$, $g_0 = 2000\,\mathrm{cm}^{-1}$, $\Gamma = 2.0$, $T_{\mathrm{loss}} = 0.98$, $R_1 = 0.999$, $R_2 = 0.98$, $A = 1.0\times10^{7}\,\mathrm{sec}^{-1}$, $B = 1.0\times10^{-10}\,\mathrm{cm}^3\mathrm{sec}^{-1}$, and $C = 6.0\times10^{-30}\,\mathrm{cm}^6\,\mathrm{sec}^{-1}$. Figure 7 shows the calculated results for the pump thresholds versus the pump-to-mode size ratio for $\mathrm{TEM}_{0,0}$ and $\mathrm{TEM}_{1,0}$ modes. For comparison, experimental data for the lasing threshold P_{th} and the critical power P_{SML} for achieving SML are also shown in figure 7. It can be seen that experimental data for the lasing threshold agree very well with the numerical results for the pump threshold of $\mathrm{TEM}_{0,0}$ mode. More importantly, experimental data for the critical power P_{SML} are also in good agreement with numerical calculations for the pump threshold of $\mathrm{TEM}_{1,0}$ mode. The good agreement confirms that the generation of $\mathrm{TEM}_{1,0}$ mode plays a critical role for the occurrence of the SML.

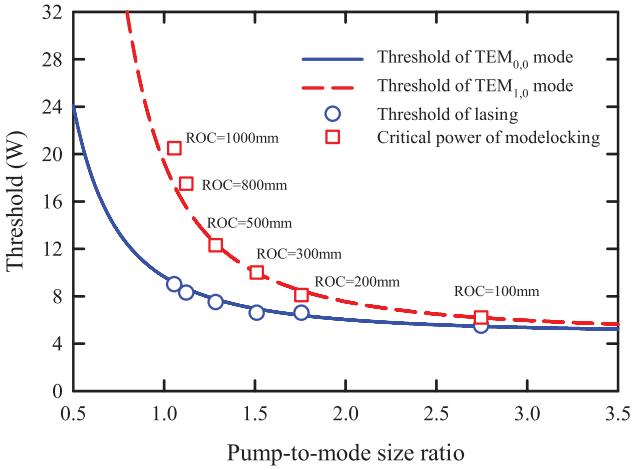

Figure 7. Calculated results for the pump thresholds versus the pump-to-mode size ratio for $\mathrm{TEM}_{0,0}$ and $\mathrm{TEM}_{1,0}$ modes and experimental data for the lasing threshold P_{th} and the critical power P_{SML} for achieving SML.

5. Conclusions

In summary, we have explored the criterion for achieving SML in an OPSL with a plano-concave cavity by using various pump-to-mode size ratios at a fixed pump radius. It has been clearly observed that the occurrence of SML is nearly synchronous with the lasing of high-order transverse modes. Since the pump threshold for high-order transverse modes significantly increases for the pump-to-mode size ratio smaller than 1.5, the critical pump power P_{SML} for achieving SML is confirmed to rise considerably. Furthermore, experimental results revealed that the continuous SML operation could not occur in the absence of high-order transverse modes. We also derived a theoretical formula with experimental parameters to calculate the pump threshold for various $\mathrm{TEM}_{n,0}$ modes. Calculated results showed that the critical pump power for obtaining the SML operation agrees very well with the pump threshold for exciting $\mathrm{TEM}_{1,0}$ mode. We believe that the present finding can provide an important guideline to explore further the SML operation in OPSLs.

Acknowledgement

The authors acknowledge the National Science Council of Taiwan for their financial support of this research under contract NSC 100-2628-M-009-001-MY3.

References

[1] Spence D E, Kean P N and Sibbett W 1991 60 fsec pulse generation from a self-mode-locked Ti:sapphire laser *Opt. Lett.* **16** 42–4

[2] Chilla J L A and Martinez O E 1993 Spatial-temporal analysis of the self-mode-locked Ti: sapphire laser *J. Opt. Soc. Am.* B **10** 638–43
[3] Cerullo G, De Silvestri S, Magni V and Pallaro L 1994 Resonators for Kerr-lens mode-locked femtosecond Ti:sapphire lasers *Opt. Lett.* **19** 807–9
[4] Cote D and van Driel H M 1998 Period doubling of a femtosecond Ti:sapphire laser by total mode locking *Opt. Lett.* **23** 715–7
[5] Bolton S R, Jenks R A, Elkinton C N and Sucha G 1999 Pulse-resolved measurements of subharmonic oscillators in a Kerr-lens mode-locked Ti:sapphire laser *J. Opt. Soc. Am.* B **16** 339–43
[6] Lin J-H, Wei M-D, Hsieh W-F and Wu H-H 2001 Cavity configurations for soft-aperture Kerr-lens mode locking and multiple-period bifurcations in Ti:sapphire lasers *J. Opt. Soc. Am.* B **18** 1069–75
[7] Liang H C, Chen R C C, Huang Y J, Su K W and Chen Y F 2008 Compact efficient multi-GHz Kerr-lens mode-locked diode-pumped Nd:YVO4 laser *Opt. Express* **16** 21149–54
[8] Liang H C, Huang Y J, Huang W C, Su K W and Chen Y F 2010 High-power, diode-end-pumped, multigigahertz self-mode-locked Nd:YVO4 laser at 1342 nm *Opt. Lett.* **35** 4–6
[9] Huang Y J, Tzeng Y S, Tang C Y, Huang Y P and Chen Y F 2012 Tunable GHz pulse repetition rate operation in high-power TEM00-mode Nd:YLF lasers at 1047 nm and 1053 nm with self mode locking *Opt. Express* **20** 18230–7
[10] Liu H, Nees J and Mourou G 2001 Diode-pumped Kerr-lens mode-locked Yb:KY(WO4)2 laser *Opt. Lett.* **26** 1723–5
[11] Lagatsky A A *et al* 2005 Yb3+-doped YVO4 crystal for efficient Kerr-lens mode locking in solid-state lasers *Opt. Lett.* **30** 3234–6
[12] Xie G Q, Tang D Y, Zhao L M, Qian L J and Ueda K 2007 High-power self-mode-locked Yb:Y2O3 ceramic laser *Opt. Lett.* **32** 2741–3
[13] Uemura S and Torizuka K 2008 Kerr-lens mode-locked diode-pumped Yb:YAG laser with the transverse mode passively stabilized *Appl. Phys. Express* **1** 012007
[14] Zhuang W Z, Chang M T, Liang H C and Chen Y F 2013 High-power high-repetition-rate subpicosecond monolithic Yb:KGW laser with self-mode locking *Opt. Lett.* **38** 2596–9
[15] Chen Y F, Lee Y C, Liang H C, Lin K Y, Su K W and Huang K F 2011 Femtosecond high-power spontaneous mode-locked operation in vertical-external cavity surface-emitting laser with gigahertz oscillation *Opt. Lett.* **36** 4581–3
[16] Kornaszewski L, Maker G, Malcolm G P A, Butkus M, Rafailov E U and Hamilton C J 2012 SESAM-free mode-locked semiconductor disk laser *Laser Photon. Rev.* **6** L20–3
[17] Albrecht A R, Seletskiy D V, Cederberg J G and Sheik-Bahae M 2013 Self-mode-locked vertical external cavity surface-emitting laser (VECSEL) *CLEO: Sci. Innov.* **2013** CW1G.5
[18] Liang H C, Lee Y C, Tung J C, Su K W, Huang K F and Chen Y F 2012 Exploring the spatio-temporal dynamics of an optically pumped semiconductor laser with intracavity second harmonic generation *Opt. Lett.* **37** 1–3
[19] Kuznetsov M, Hakimi F, Sprague R and Moodadian A 1999 Design and characteristics of high-power (>0.5-W CW) diode-pumped vertical-external-cavity surface emitting semiconductor lasers with circular TEM00 beams *IEEE J. Sel. Top. Quantum Electron.* **5** 561
[20] Chen Y F, Huang T M, Kao C F, Wang C L and Wang S C 1997 Generation of Hermite-Gaussian modes in fiber-coupled laser-diode end-pumped lasers *IEEE J. Quantum Electron.* **33** 1025–31